

PAPER • OPEN ACCESS

The impact of hydrogen plasma on the structure and morphology of tin and lead micrometer sized particles

To cite this article: D Shefer *et al* 2023 *J. Phys. D: Appl. Phys.* **56** 085204

View the [article online](#) for updates and enhancements.

You may also like

- [Improving the photovoltaic performance of the all-solid-state TiO₂/NR/CuInS₂ solar cell by hydrogen plasma treatment](#)
Bingfeng Chen, Wenzhe Niu, Zirui Lou et al.
- [Erosion research of CX-2002U carbon composites under low-temperature high-flux hydrogen plasma](#)
Hengxin GUO, , Zongbiao YE et al.
- [Anisotropic selective etching between SiGe and Si](#)
Yohei Ishii, Ritchie Scott-McCabe, Alex Yu et al.

The impact of hydrogen plasma on the structure and morphology of tin and lead micrometer sized particles

D Shefer^{1,*} , A Nikipelov², M van de Kerkhof², Z Marvi², V Banine^{1,2} and J Beckers¹ 

¹ Eindhoven University of Technology, Department of Applied Physics, Eindhoven 5600 MB, The Netherlands

² ASML, Veldhoven 5504 DR, The Netherlands

E-mail: d.shefer@tue.nl

Received 2 May 2022, revised 19 December 2022

Accepted for publication 17 January 2023

Published 8 February 2023



CrossMark

Abstract

The stability of micrometer sized particles in hydrogen plasma is essential for extreme ultraviolet lithography, the ITER fusion program and the application of hydrogen plasma etching. We experimentally investigated the morphological evolution of tin (Sn), lead (Pb), and lead (II) oxide (PbO) micrometer sized particles on a surface that is exposed to a low pressure hydrogen plasma. Post exposure particle cross sections obtained by a scanning electron microscope accompanied by a focused ion beam demonstrated a significant influence of hydrogen plasma exposure on both the surface and the bulk material of the particles. Chemical sputtering at the surface and accumulation of pressurized hydrogen bubbles in cavities in the bulk material are the main drivers of the morphological changes. These mechanisms may influence the adhesion of particles to the surface through the introduction of asperities, increase of contact spot area, or fragmentation after the accumulation of mechanical stress.

Keywords: EUV plasma, hydrogen plasma, contamination, tin, lead, particles

(Some figures may appear in colour only in the online journal)

1. Introduction

The retention of particles on a surface in a hydrogen plasma environment is important for technologies with contamination control, such as extreme ultraviolet (EUV) lithography [1–3], the ITER fusion program [4–6], and plasma-enhanced catalytic activation [7]. All these technologies are sensitive to particles in the size range from approximately 20 nm up to a micrometer. Furthermore, hydrogen plasma etching might replace halogen etching in semiconductor manufacturing as it

is believed to be less aggressive and does not etch a too extensive range of materials as halogens do [8].

EUV lithography enables the shrinkage of devices in the semiconductor industry and improves the cost and energy efficiency of integrated circuits. However, the total yield of the production of integrated circuits is adversely affected by contamination, i.e. the deposition of particles on critical surfaces, such as a reticle or wafer. EUV radiation with the wavelength of 13.5 nm ionizes the low pressure H₂ in litho-scanners and generates a low temperature and low density plasma used to clean EUV optics [9–13]. EUV-induced hydrogen plasma was found to enhance particle release from surfaces and to increase particle transport to critical surfaces [14]. For instance, tin (Sn) contaminants are traced back to Sn-based EUV source [15]. The proposed mechanisms for the enhancement of contamination include the production of solid hydrides at the surface of the particle or hydrogen-filled pressurized cavities inside

* Author to whom any correspondence should be addressed.



Original Content from this work may be used under the terms of the [Creative Commons Attribution 4.0 licence](https://creativecommons.org/licenses/by/4.0/). Any further distribution of this work must maintain attribution to the author(s) and the title of the work, journal citation and DOI.

of the particles, both accompanied by accumulation of mechanical stress that can result in particles' deformation or fragmentation. Alternatively, ion or radical-induced etching of the particles may introduce (or amplify) asperities and result in the gradual loss of the adhesion, enabling particles' release [16].

It has been long understood that the transport of dust particles is a major safety issue for ITER and future fusion devices, owing to the possibility of radioactive or toxic dust release to the atmosphere upon loss of vacuum accidents [17]. Moreover, dust transport has been consistently observed in tokamaks [18]. Toliás *et al* broadly described the effect of dust transport in the ITER fusion reactor and concluded that the effect of nano-asperities due to morphological changes appearing during plasma operations is one of the main factors causing particles' mobilization [4]. The damaged surface of the reactor wall (the tungsten foam) was demonstrated by Brezinsek *et al* [5]. Atomic and ionic deuterium and tritium damaging tungsten by physical sputtering, ion implantation and trapping of molecular deuterium and tritium under the surface may be approximated to an extent by the low temperature hydrogen plasma damaging tin and lead, which is reported in this work.

Hydrogen plasma may improve semiconductor etching processes [7]. The etching of semiconductors, metals, and insulators requires gas mixtures containing halogens and their compounds. Such etch mixes are effective, yet hydrogen plasma forms volatile hydrides with some of the relevant materials and may have some benefits in terms of selectivity for etching as a milder instrument [8]. Considering the adverse effect of contaminants on semiconductor yield, one should improve understanding of particle generation and mobilization mechanisms in hydrogen plasma in such environments.

Materials chosen for the study of this paper are relevant for EUV lithography or have high sensitivity to chemical sputtering and atomic hydrogen-induced transport. Sn, lead (Pb) and lead (II) oxide (PbO) form volatile hydrides (e.g. stannane SnH₄, plumbane PbH₄ and H₂O) at room temperature when exposed to H₂ plasma; moreover, they have high diffusion coefficient for atomic hydrogen and low diffusion coefficient for molecular hydrogen, which is expected to enhance the formation of pressurized H₂ cavities.

Because industrial applications rely on process cleanliness, understanding the plasma influence on particle generation or mobilization is of critical importance. The current work demonstrates the morphological changes of tin and lead micrometer sized particles under exposure to a low pressure hydrogen plasma, suggests underlying mechanisms and the possible impact of such mechanisms on adhesion and in extreme cases on particle fragmentation.

2. Experimental methods

The experiments were carried out in three steps. First, non-spherical particles of Sn, Pb or PbO (yellow) from SigmaAldrich™ with an indicated size distribution of 1–30 μm were mechanically dispersed on a 1 inch sapphire wafer covered with a 100 nm thick Cr coating. Second, the samples were

exposed to hydrogen plasma with various doses and constant ion flux and energy. The samples were divided into several groups by their exposure time: from nil (virgin, without being exposed) to 70 h of H₂ plasma exposure with one wafer exposed at a time. Third, cross-sections of the particles were analyzed in a scanning electron microscope/focused ion beam (SEM/FIB). It should be noted that air exposure between plasma exposure and analysis was unavoidable in the current experiments, and the particles could be partially oxidized.

2.1. ECR hydrogen plasma setup

Figure 1 shows a schematic drawing of the plasma vessel used in the experiments. Hydrogen plasma chosen for the experiments represents the conditions of the afterglow of the EUV-induced hydrogen plasma with a boost factor. The EUV plasma fluxes of ions and radicals require hundreds of hours of exposure to cause particle release in the vicinity of critical surfaces [9]. Having a hundredfold more intense flux and approximately 5 times higher energy of the ions compared to the EUV-induced plasma [19], the experiment conditions are expected to accelerate the effects on the particles by approximately 100 times. Working with low pressures, temperatures and under supersaturation conditions of dissolved hydrogen, we assume the scaling is reasonable [20]. The hydrogen plasma was driven by an electron cyclotron resonance (ECR) plasma source [21] Aura-Wave™ from Sairem exhausting into a vessel of 20 × 20 × 20 cm³ in size. The sample faced the plasma head and was located 10 cm apart in the middle of the vessel. The sample holder and the sample were connected to the rest of the vessel and served as ground. Hydrogen was supplied at 20 sccm into the chamber and evacuated by a turbo molecular pump (Pfeiffer THU 200 MP) connected to a scroll dry pre-pump (Edwards XDS10). The pressure inside the chamber was monitored by Philips vacuum gauges (HPT 200 Pirani/Bayard–Alpert and PPT 200 AR, both hydrogen calibrated). Before samples were exposed to the plasma and without hydrogen supply, a base pressure of less than 10^{−4} Pa was obtained. The plasma was maintained at 5 Pa pressure with 100–200 W input RF power at 13.56 MHz in an automatically adjusting the resonance frequency mode (tuning mode). During plasma exposures the sample temperature remained in the range from 20 °C to approximately 60 °C.

The ECR source produces a low-temperature plasma with a smooth distribution of the plasma characteristics, e.g. plasma density and electron temperature decays with distance from the source. Values for the electron temperature $T_e \cong 5$ eV and density $n_e \sim 10^{16} \text{ m}^{-3}$ were used from Shirai *et al* [21]. From those parameters, it is estimated that the substrate was exposed to a uniform flux of ions of about $I = \sim 10^{15} \text{ cm}^{-2}$ (1 Am^{−2}) with energies obtained in the plasma sheath of about $E_i = 2 - 3 \times T_e$ or 10–15 eV. The radical flux was 10–100 times higher than the ion flux due to 1–10% chance of radical association at stainless steel walls of the main vacuum chamber, compared to 100% chance of ion recombination.

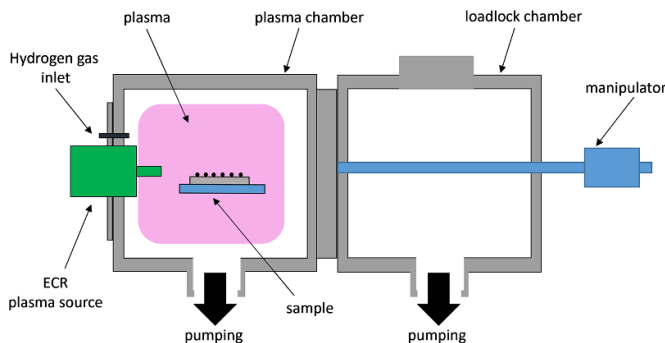


Figure 1. Schematic drawing of the experimental setup. The setup comprised the main vessel and the loadlock chamber, separated by a gate valve. The sample with deposited micrometer sized particles was mounted in the main vessel facing (and 10 cm apart from) the ECR plasma head.

2.2. SEM/FIB measurements

Prior and post-exposure to H_2 plasma, the particles were examined in a SEM/FIB (NovaNanolab 600i). The SEM images comprising the top view of the particles were reported earlier in our previous work [1]. Hereby we report on the addition of SEM images of the particles' cross-sections produced by an ion beam. In order to reduce damage, carbon deposition, heating, and sputtering by electron and ion beams, the SEM/FIB parameters were set to minimal values: SEM beam energy was limited to 10 kV and current to 0.4 nA, FIB Ga ion beam energy was limited to 10 kV and current to 0.46 nA.

3. Results

The results section of this paper is divided into three subsections according to the corresponding type of particles: tin, lead, and lead monoxide. Each section contains the SEM/FIB cross sections of particles prior and post exposure to the plasma to various doses. Per subsection, we provide suggestions for the possible damaging mechanism(s). The samples and the exposure times are listed in the table 1.

3.1. Exposure of tin particles to H_2 plasma

Tin particles exposed to hydrogen plasma show a significant change with respect to both surface and bulk properties (figure 2). As can be seen from figures 2(b) and (c), tin particles under high plasma load develop bubbles in their bulk material and spikes at their surface. The number of these structural changes appears to increase with the exposure time. Interestingly, the bubbles are non-spherical and tend to be shaped along a body-centered tetragonal lattice. The typical size of these plasma-induced structures ranges from a few tens of nm to a few tens of micrometers. One explanation for the appearance of these H_2 bubbles is that they build up at interstitial sites in the host lattice and crystal defects, playing a role of a sink for hydrogen atoms. Jumping between neighboring interstitial sites hydrogen atoms can diffuse over a big distance from the surface [20].

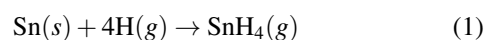
Table 1. The plasma exposure time and applied power of the samples.

| Material | Exposure time (RF power) | | |
|----------------|--------------------------|------------|-------------|
| Sn (figure 2) | 0 h | 7h (150 W) | 70h (100 W) |
| Pb (figure 4) | 0 h | 3h (200 W) | 18h (100 W) |
| PbO (figure 5) | 0 h | 3h (200 W) | 18h (100 W) |

Low energy hydrogen ion implantation is limited only to a few nm. Ions are incident normal to the substrate, while bubbles are, obviously, evenly distributed across the Sn particle's volume. This indicates the diffusive nature of the process (while ion implantation may be more relevant in the ITER divertor damaging), and the significance of the role of hydrogen atoms supplied to a particle from every direction. Reactions with radicals and ions, relevant for etching are barrier-free reactions. In this case the Gibbs free energy (ΔG°) fully defines kinetics of the reaction. For a molecule to be unstable, the decomposition reaction Gibbs energy must be negative and negativity determines the decomposition rate of the molecules.

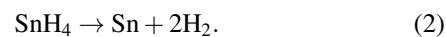
The bubbles, with trapped hydrogen pressure approaching the ultimate tensile strength (UTS) of tin, which is 220 MPa [22], grow along the crystalline planes. The explosion or burst of such bubbles may cause the fragmentation or release of the particles from the surface exposed to plasma, and so this effect must be accounted in applications that are critical with respect to defectivity.

Spikes at the surface in figure 2(c) likely correspond to the formation/decomposition of stannane (SnH_4) as reported by Tamaru [23]. Stannane is a gas at room temperature [24] for which the formation reaction with hydrogen radicals is endothermic with the standard entropy energy ΔS° and enthalpy ΔH° at 298 K being equal to $-282 \text{ JK}^{-1} \text{ mol}^{-1}$ and $-709.2 \text{ kJ mol}^{-1}$, respectively (table 2). This yields a total $\Delta G^\circ = -625.2 \text{ kJ mol}^{-1}$. The formation of stannane upon the interaction between tin and hydrogen radicals follows the reaction



where *s* and *g* indicate the surface and gas phase respectively. The reaction with molecular hydrogen is exothermic and, thus, less likely.

According to our calculations, the decomposition of stannane on catalytically active surface proceeds spontaneously with the corresponding Gibbs free energy of $\Delta G^\circ = -187.8 \text{ kJ mol}^{-1}$ (which is close to those, reported by Ugur *et al* [25]). Using x-ray photoelectron spectroscopy the authors confirmed the decomposition of stannane on a metal surface into pure metallic tin by



In this respect, Ugur *et al* suggested a possible mechanism for the decomposition of SnH_4 under various hydrogen fluxes (ranging from 5.4×10^{16} to $3.2 \times 10^{17} \text{ cm}^{-2} \text{ s}^{-1}$). The author argued that for low radical flux ($\sim 5 \times 10^{16} \text{ cm}^{-2} \text{ s}^{-1}$)

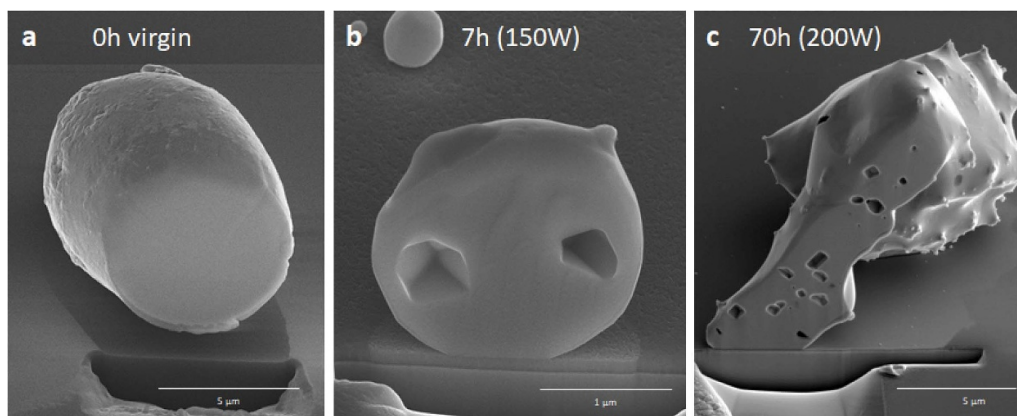


Figure 2. SEM images of tin micrometer sized particles' cross-sections after exposure to hydrogen plasma. From left to right by exposure time: not exposed (a), 7 h of exposure at 150 W (b), 70 h of exposure at 200 W (c).

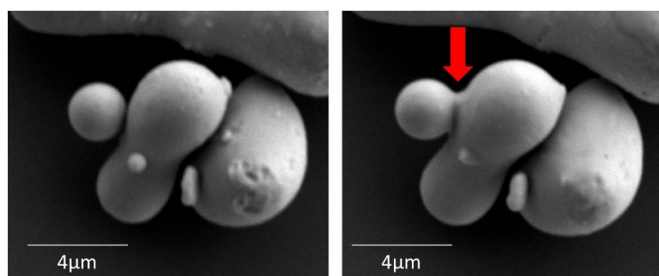


Figure 3. SEM images of tin particles particle before (on the left) and after 1.5 h of exposure to hydrogen plasma at 100 W (on the right), during exposure tin remained below the melting point. The arrow indicates the emerging bridge between the particles, confirming tin transfer along the particle surface.

the majority of atoms will likely recombine on the surface into H_2 molecules with only a few of them interacting with Sn as was suggested in the similar study on Ru and resulting in the low etching rate [26]. At higher flux $\sim 3 \times 10^{17} \text{ cm}^{-2} \text{ s}^{-1}$, corresponding to conditions similar to our experiments ($\sim 10^{17} \text{ cm}^{-2} \text{ s}^{-1}$), the efficiency of the reaction of impinging radicals H with Sn is growing as more H_2 molecules desorb and more Sn spots on the surface is available. This means the suggested mechanism of surface mass transfer is reliable.

The catalytic activity of the tin's surface for stannane seems to be higher compared to the wafer's surface coated with native oxide Cr_2O_3 . The figure 3 shows the surface migration of tin atoms between two physically connected particles, making a bridge. The effect was achieved already after 1.5 h of exposure to the plasma. We did not observe such effects on the particles, separated by a gap of the wafer surface. Furthermore, the original particle was rough as can be seen in figure 2(a). The exposed Sn particle in figure 2(c) is smoother except for individual spikes, which also supports our hypothesis of tin transport along the particle surface in a cycle of formation and decomposition of stannane. In addition, for some tin particles after exposure, we also observed the increased contact spot area to the Cr-coated wafer (figures 2(b) and (c)), which is

unexpected for pristine aspherical particles. With this, we can conclude the plasma-induced surface tin transfer contributes to the growing adhesion force over time of exposure. It is in contrast to commonly reported the effect of reducing the van der Waals force.

3.2. Exposure of lead particles to H_2 plasma

Similarly to tin, the formation of a lead hydride is very likely. Plumbane (PbH_4) was reported by many authors as a very unstable hydride and it lacks accurate measurements [27, 28]. In table 2 we assessed plumbane's formation and decomposition ΔG° by extrapolating the enthalpies ΔH° of the similar reactions with C, Si, and Sn. Indeed, plotting enthalpies of the hydride formation/decomposition of the reactions listed in table 2 versus their bond energies C–H, Si–H, Sn–H and Pb–H (337 kJ mol^{-1} , 300 kJ mol^{-1} , 267 kJ mol^{-1} and 176 kJ mol^{-1} respectively) [29], the formation and decomposition enthalpies of plumbane can be assessed to -405 kJ mol^{-1} and -460 kJ mol^{-1} respectively. As can be seen, the entropies of the reaction are nearly equal. Assuming the entropies for plumbane reactions as for stannane (-282 J mol^{-1} and 84 J mol^{-1} respectively), the Gibbs free energy was calculated.

Plumbane, being formed in the reaction



is much less stable compared to stannane molecule [30], confirmed by the strong negativity of the assessed ΔG° reaction. Thus, the plumbane is likely to decompose on the surface before having a chance to leave it, and the redeposition of lead is even more likely than the redeposition of tin (figure 4). Though, the assessed ΔG° of stannane production is more negative compared to plumbane (which translates into the higher etching speed for tin), from the figure 4 we can conclude that lead's morphology changes faster than tin's. Therefore, the dominant mechanism for Pb morphology evolution is the formation of bubbles. The bubbles inflate and rupture near the surface (figure 4(c)), which explains the seemed 'etching' effect.

Table 2. The Gibbs free energy, entropy and enthalpy of the formed and decomposed volatile hydrides given at 298 K. The data for materials interacting with hydrogen is given for solid bodies. Formation and decomposition of plumbane (PbH_4) was empirically assessed based on the stannane (SnH_4) data.

| Reaction | ΔG° kJmol^{-1} | ΔH° kJmol^{-1} | ΔS° $\text{JK}^{-1}\text{mol}^{-1}$ | References |
|---|--------------------------------------|--------------------------------------|--|------------|
| $\text{C} + 4\text{H} \rightarrow \text{CH}_4$ | -864.7 | -946.9 | -276 | [24, 41] |
| $\text{CH}_4 \rightarrow \text{C} + 2\text{H}_2$ | 50.7 | 74.9 | 81 | [24, 41] |
| $\text{Si} + 4\text{H} \rightarrow \text{SiH}_4$ | -757.0 | -837.5 | -270 | [24, 41] |
| $\text{SiH}_4 \rightarrow \text{Si} + 2\text{H}_2$ | -46.2 | -34.3 | 40 | [24, 41] |
| $\text{Sn} + 4\text{H} \rightarrow \text{SnH}_4$ | -625.9 | -709.2 | -282 | [24] |
| $\text{Sn} + 2\text{H}_2 \rightarrow \text{SnH}_4$ | 187.8 | 162.8 | -84 | [24] |
| $\text{SnH}_4 \rightarrow \text{Sn} + 2\text{H}_2$ | -187.8 | -162.8 | 84 | [24, 25] |
| $\text{Pb} + 4\text{H} \rightarrow \text{PbH}_4$ | -321.0 | -405.0 | -282 | assessed |
| $\text{PbH}_4 \rightarrow \text{Pb} + 2\text{H}_2$ | -485.0 | -460.0 | 84 | assessed |
| $\text{PbO} + 2\text{H} \rightarrow \text{Pb} + \text{H}_2\text{O}$ | -455.0 | -503.7 | -160 | [24, 42] |

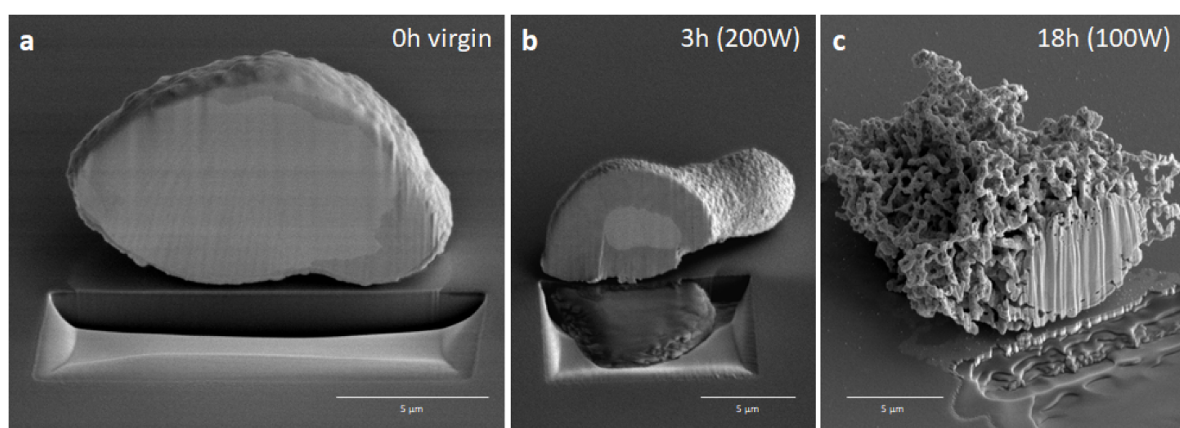


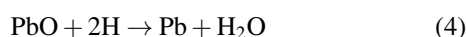
Figure 4. SEM images of lead micrometer sized particles' cross-sections after exposure to hydrogen plasma. From left to right by exposure time: not exposed (a), 3 h of exposure at 200 W (b), 18 h of exposure at 100 W (c).

The different phases within the lead particles' cross sections can be associated with lead's response to the electron beam. The pristine particle (figure 4(a)) may have a native oxide shell with a different density which seems darker in the SEM images. The hydrogen exposed particles (see figures 4(b) and (c)) appear to have a hydrogen-rich zone which appears as a dark area, whereas the pristine (hydrogen-free) lead area appears brighter.

3.3. Exposure of lead (II) oxide particles to H_2 plasma

Lead (II) oxide particles demonstrate even the fastest change when exposed to hydrogen plasma compared to the tin and lead particles (see figure 5).

Note that the retrieving of oxygen, occurring in the reaction



is a more likely process than plumbane formation, since fewer reactants are needed to form it and since the water formation Gibbs free energy (-237.1 according to Dean [31]) is more negative than, for instance, plumbane formation ΔG° . Thus, the dominant process in PbO particles is etching and it is likely to proceed via $\text{PbO} \rightarrow (\text{partialoxide}) \rightarrow \text{Pb} \rightarrow \text{PbH}_4$. The low density partial oxide will yield a low density lead that in turn is easier to etch or blister due to the abundance of active sites.

4. Discussion

We can classify various cases of hydrogen interaction with the particles based on the observations. The particle may be subjected to three independent mechanisms: etching, bubble formation, and physical sputtering. Some properties of the materials must be considered, when evaluating the dominant mechanism: formation/decomposition rate of the hydrides (if present), diffusion properties of hydrogen atoms in the particle, and the material's UTS. The diffusion of radicals was studied only in C and Si. There is a lack of information about diffusion in Sn, Pb, and PbO .

4.1. Etching and surface mass transfer

The ability of some materials to form volatile hydrides determines the possibility of etching those materials in hydrogen plasma, and consequently the chance of material transfer in the cycle of formation and decomposition of hydrides. The stability of volatile hydrides decreases moving from C to Pb within the fourth group of the periodic table along with the formation of the Gibbs free energy (table 2). It is likely that hydrides from C to Si are so stable that redeposition and material transfer are insignificant. Sn hydride is intermediate in its stability, so the material transfer is noticeable. Pb hydride is

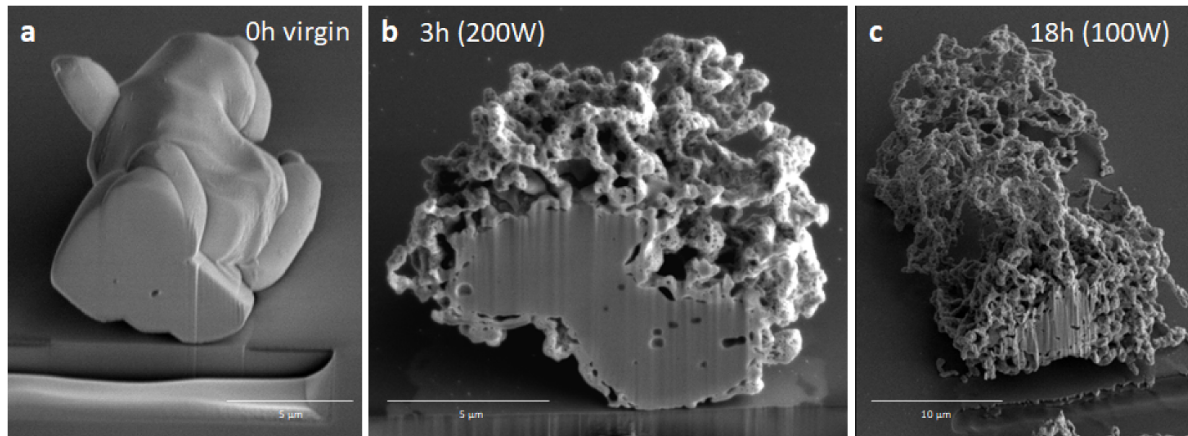


Figure 5. SEM images of lead oxide micrometer sized particles' cross-sections after exposure to hydrogen plasma. From left to right by exposure time: not exposed (a), 3 h of exposure at 200 W (b), 18 h of exposure at 100 W (c).

so unstable that material transfer is likely happening on the small scale, possibly smaller than the particle itself. Pb is not on the list, as plumbane may even decompose before it diffuses far from the surface. However, PbO is etchable, because of the oxygen extraction by the plasma. As an example, dry etching of Si in hydrogen and halogen-containing plasmas was widely studied [32]. The etching of C by hydrogen plasma was assessed by Park to 0.1 nm min^{-1} at room temperature [33]. Carbon etching in EUV plasma was calculated by Astakhov and van Leuken, resulting both in about 0.3 nm min^{-1} [34, 35]. The etching of amorphous Si by hydrogen plasma was found to be of an order of 1 nm min^{-1} [36]. The etching of Sn by hydrogen radicals in EUV-induced plasma applications was studied by van Herpen *et al* [37], resulting in etch rates of about 50 nm min^{-1} on a silicon substrate and 28 nm min^{-1} on a Ru substrate. The etching of Sn particles by hydrogen plasma was described by Elg *et al* [38], with etch rates at room temperature of about $1\text{--}10 \text{ nm min}^{-1}$ for typical capacitively coupled plasma or typical conditions for hydrogen radical generators. There is no literature data regarding lead etching by hydrogen plasma.

Surface migration of tin atoms by formation and decomposition of stannane is significant for both: the particle's shape and the region of contact (translated into the particle's adhesion force). The exposed tin particle presented the increased plane-to-plane contact area, which is unexpected as typically plasma is known to suppress the van der Waals force by inducing nanoasperities. For contamination control, it might be relevant to investigate which of the processes wins: the emerging spikes increasing the particle/substrate separation and promoting the release or the increasing sticking coefficient, preventing the particle from release. The mechanism of surface migration seems to be important for materials with unstable volatile hydrides. As a result, such an effect was not reported for silicon, i.e. the silane molecule is stable and does not decompose near the particle. However, in our experiments, we did not observe the increased contact spot for lead particles that could confirm the trend, presumably due to the dominant bubbles rupturing near the surface.

Due to the lack of reliable information regarding the etching of lead and lead oxides by hydrogen plasma, we will refer to our experiments and the previous publication [1]. As was demonstrated before, lead oxide has a higher tendency toward etching (figure 5) because of the production of water. Etching-induced asperities or stress-induced dislocations in subsurface layers may impede the diffusion of atomic hydrogen deeper into the bulk by trapping it and so promote bubbles near the surface and suppress bubbles in the bulk.

4.2. Bubble inflation/particle fragmentation

Trapping of H_2 under the particle's surface in bubbles and subsequent particle fragmentation may occur even if the incident energy of ions is too low to create a physical displacement. The atomic or ionic hydrogen from the plasma adsorbs on a surface or near the surface (some nm after implantation), diffuses into the bulk, and precipitates on low energy sites such as cavities and vacancy clusters or dislocations. The recombination of hydrogen atoms to H_2 in such cavities or at such vacancy sites leads to the accumulation of H_2 gas at increasing pressure and deformation. This eventually leads to the formation of blisters (f.i., figure 2(c)). Growing blisters are associated with stress, centered on the blister (see figure 6, the enlarged scheme) which exponentially relaxes towards the surface of the particle.

As shown in the figure 6, blister growth depends on the relative rates of hydrogen supply by diffusion process to and escape from the cavity and on the equilibrium between molecular and atomic hydrogen densities locally [14, 39]. If outgassing exceeds the supply of hydrogen, the blister will collapse.

The rate of hydrogen supply to the cavity depends on bulk diffusion properties and on the occupancy of sites on the surface. The dissolved hydrogen atoms energetically tend to accumulate into bubbles on vacancy defects and near dislocations. The bubbles distribution is determined not only by the diffusion length of hydrogen atoms but also by screening effects of defects and existent bubbles. For instance, the higher diffusion coefficient for lead compared to tin is compensated by

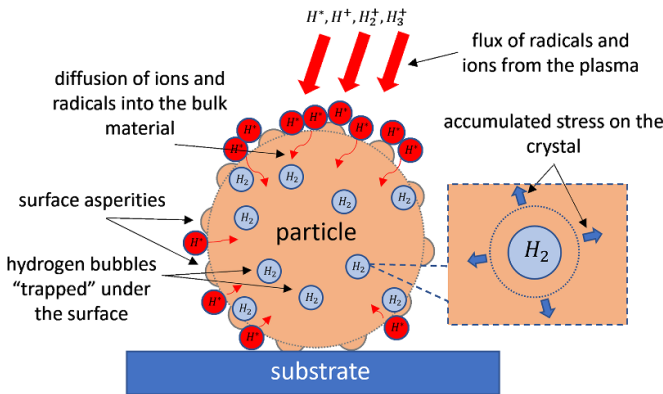


Figure 6. An illustration of a particle exposed to hydrogen plasma and a schematic displaying the propagation of atomic hydrogen within the crystal, i.e. the diffusion of hydrogen radicals to low-energy sites such as cavities or crystal defects. The pointed spots promote the formation of molecular hydrogen leading to an increased hydrogen pressure locally.

a larger number of dislocations (the number of dislocations is inversely proportional to the material’s UTS [40]), so in lead (and in partial lead oxide) bubbles are concentrated in the layer at a fraction of a micrometer from the particle surface. In tin, as expected, the bubbles are distributed evenly in the bulk, which indicates that diffusion spreads atomic hydrogen concentration only after the precipitation takes place.

In order to form a blister or even a bubble, some conditions must be fulfilled. First, materials with high enthalpy of solution ΔH and, as consequence, with a high concentration of dissolved hydrogen (when subjected to hydrogen plasma) are naturally prone to bubble formation [20]. Alternatively if H dissolution is a barrier reaction, ion implantation should promote saturation of the bulk. Second, the diffusion of radicals must be sufficient to supply atomic hydrogen to the emerging bubble faster than outgassing that tries to deflate it. Hydrogen radicals, as was discussed before, diffuse in metals by jumping between interstitial sites. It was found that the dense packing of the silicon structure enabled an H incorporation depth of only about 10 nm under incident energies of 300 eV and once implanted, atomic hydrogen stayed in place. That means that the formation of blisters in silicon is excluded and etching is dominant. Third, the mechanical properties of the particle must be taken into account. The pressure inside of the growing bubble exceeds UTS, so materials with low UTS also prone to bubble formation.

Condon proposed three basic criteria in order to conclude if the blisters appear to qualify for growth [43]. The first criterion is the supersaturation of dissolved hydrogen. The rest of the criteria depend on the level of hydrogen supersaturation. In cases where the saturation is under a certain threshold, the additional criterion of vacancy supersaturation is needed. To make this mechanism possible, the concentration of metal vacancies must be greater than expected for the equilibrium state. This may happen in the presence of impurities or crystal defects. The upper limit of supersaturation determines whether the process goes to the formation of cavities or to the formation of hydrides. This criterion says that the supersaturation

level must remain below the concentration for hydride formation. The supersaturation effect was also observed by Ou and co-authors [44]. As an example, for instance, the research of Kamada related to hydrogen implantation in aluminum [45].

Xie *et al* [46]. showed that, in general, the growth of a blister near the surface begins with the appearance of a nano-scale gas bubble (with a certain radius of curvature R), promoted by the internal gas pressure P , plastically deforms the covering layer that becomes visible on a particle’s surface in SEM. Based on their review for hydrogen blistering in aluminum, the pressure P within this blister with saturated hydrogen must exceed the yield strength σ_Y of the material in covering layer and its surface energy γ . The critical blister radius R_C before explosion depends on P with the following relationship [46]:

$$P - \frac{4\sigma_Y t^2}{3R_C^2} - \frac{2\gamma}{R_C} > 0 \quad (5)$$

where t denotes the thickness of the capping layer. Using the values (220MPa, 0.5×10^{-6} m, 0.5×10^{-6} m, 10^{-9} Jm $^{-2}$) for the given parameters (σ_Y , R_C , t and γ) respectively, which are typical in these experiments, the pressure within the bubble reaches of about 290MPa that exceed the material’s yield strength and therefore corresponds with the observations.

4.3. Physical sputtering damage

The maximum momentum transfer in a collision between the heaviest hydrogen-ion (H_3^+) in the ECR hydrogen plasma used in this work and the lightest target element (Sn) with a bond energy of about 3 eV is limited to 10% with a total threshold for ions of around 25 eV. Therefore, the effect of physical sputtering by hydrogen ions can be neglected [14].

One should note here that, probably, all the damaging processes listed above might act on each of the chosen materials collectively. However, the bulk properties dictate which mechanism is dominant. The relative sensitivities of Pb and PbO particles to hydrogen plasma compared to that of Sn particles is denoted by the decreasing stability of their hydrides as moving down in the periodic table (from carbon to lead). As discussed in this section, the increasing stability of hydrides at hydrogen supersaturation conditions decreases blister formation and promotes chemical etching. Furthermore, the low yield strength of 16–17 MPa [47] for Pb and PbO compared to 220 MPa for Sn particles means a much lower pressure inside the bubbles is required to enable bubble inflation in these low yield strength materials. However, the bubbles are barely formed deep in the bulk of Pb and PbO particles as atomic hydrogen precipitate on the abundant dislocations and lattice defects, more concentrated in Pb and PbO (partially reduced, stressed), compared to Sn.

5. Conclusions

Tin, lead and lead (II) oxide particles exposed to hydrogen plasma were investigated using SEM in combination with FIB.

The core objective of this study is elucidation of the plasma interaction with the selected particles.

With the obtained results we confirm that reactive materials (subjected to etching or trapping of molecular hydrogen under the surface) in hydrogen or EUV plasmas may impact the adhesion. The adhesion alteration is associated with two mechanisms. In the first mechanism the surface mass transfer leads to the morphology change and increased contact area between the particle and the substrate. The second mechanism is the rupture of blisters that is associated with particle fragmentation.

We found that despite the different energies, the mechanism of chemical sputtering in lead is similar to the tungsten foam production in the ITER reactor.

In order to use hydrogen plasma as a tool for selective etching we advise avoiding the materials with a high coefficient of atomic hydrogen diffusion due to the bubbling inflation in the bulk and their subsequent rupture.

Data availability statement

The data that support the findings of this study are available upon reasonable request from the authors.

Acknowledgment

The assistance of B C Barcones in the FIB measurements, P Sanders, A B Schrader, J T Kohlhepp in technical questions, as well as ASML in financial and scientific support is gratefully acknowledged.

ORCID iDs

D Shefer  <https://orcid.org/0000-0001-9179-5555>

J Beckers  <https://orcid.org/0000-0001-6116-7013>

References

- [1] Shefer D, Nikipelov A, van de Kerkhof M, Banine V and Beckers J 2021 Morphology change and release of tin and lead micro-particles from substrates in hydrogen plasma *Proc. SPIE* **11609** 116091F
- [2] van Es R *et al* 2018 EUV for HVM: towards an industrialized scanner for HVM NXE3400B performance update *Extreme Ultraviolet (EUV) Lithography IX* vol 10583, ed K A Goldberg (San Jose, CA: SPIE Advanced Lithography) pp 102–13
- [3] Beckers J, van de Ven T, van der Horst R, Astakhov D and Banine V 2019 EUV-induced plasma: a peculiar phenomenon of a modern lithographic technology *Appl. Sci.* **9** 2827
- [4] Toliás P *et al* 2016 Dust remobilization in fusion plasmas under steady state conditions *Plasma Phys. Control. Fusion* **58** 025009
- [5] Brezinsek S *et al* 2017 Plasma–wall interaction studies within the EURO fusion consortium: progress on plasma-facing components development and qualification *Nucl. Fusion* **57** 116041
- [6] Peillon S *et al* 2020 Dust sampling in WEST and tritium retention in tokamak-relevant tungsten particles *Nucl. Mater. Energy* **24** 100781
- [7] Cojocaru C, Senger A and Le Normand F 2006 A nucleation and growth model of vertically-oriented carbon nanofibers or nanotubes by plasma-enhanced catalytic chemical vapor deposition *J. Nanosci. Nanotechnol.* **6** 1331–8
- [8] Chang R, Chang C and Darack S 1982 Hydrogen plasma etching of semiconductors and their oxides *J. Vac. Sci. Technol.* **20** 45–50
- [9] van de Kerkhof M A, Yakunin A, Kvon V, van de Wetering F, Cats S, Heijmans L, Nikipelov A, Lassise A and Banine V 2020 Understanding EUV-induced plasma and application to particle contamination control in EUV scanners *Proc. SPIE* **11323** 113230Y
- [10] van der Velden M H L, Brok W J M, van der Mullen J J A M and Banine V 2006 Kinetic simulation of an extreme ultraviolet radiation driven plasma near a multilayer mirror *J. Appl. Phys.* **100** 073303
- [11] van der Horst R M *et al* 2016 Exploring the electron density in plasma induced by EUV radiation: I. experimental study in hydrogen *J. Phys. D: Appl. Phys.* **49** 145203
- [12] van der Horst R M, Osorio E A, Banine V Y and Beckers J 2015 The influence of the EUV spectrum on plasma induced by EUV radiation in argon and hydrogen gas *Plasma Sources Sci. Technol.* **25** 015012
- [13] Astakhov D I *et al* 2016 Exploring the electron density in plasma induced by EUV radiation: II. numerical studies in argon and hydrogen *J. Phys. D: Appl. Phys.* **49** 295204
- [14] van de Kerkhof M A, Galutschek E, Yakunin A, Cats S and Cloin C 2020 Particulate and molecular contamination control in EUV-induced H₂-plasma in EUV lithographic scanner *Proc. SPIE* **11489** 114890K
- [15] van de Kerkhof M A, van Empel T, Lercel M, Smeets C, van de Wetering F, Nikipelov A, Cloin C, Yakunin A and Banine V E 2019 Advanced particle contamination control in EUV scanners *Proc. SPIE* **10957** 109570U
- [16] Jaiswal R P and Beaudoin S P 2011 Nanoparticle adhesion models: applications in particulate contaminant removal from extreme ultraviolet lithography photomasks *J. Adhes. Sci. Technol.* **25** 781–97
- [17] Van Dorselaere J-P, Perrault D, Barrachin M, Bentaib A, Bez J, Cortès P P, Seropian C, Trègourès N and Vendel J 2009 R&D on support to ITER safety assessment *Fusion Eng. Des.* **84** 1905–11
- [18] Roche H *et al* 2011 First results from dust detection during plasma discharges on tore supra *Phys. Scr.* **T145** 014022
- [19] van de Ven T H M, Reefman P, de Meijere C A, van der Horst R M, van Kampen M, Banine V Y and Beckers J 2018 Ion energy distributions in highly transient EUV induced plasma in hydrogen *J. Appl. Phys.* **123** 063301
- [20] Kirchheim R and Pundt A 2014 Hydrogen in metals *Physical Metallurgy* (Amsterdam: Elsevier) p 25972705
- [21] Shirai K, Iizuka T and ichi Gonda S 1989 Electric probe measurements in an ECR plasma CVD apparatus *Jpn. J. Appl. Phys.* **28** 897–902
- [22] Kaye G W C 1986 *Tables of Physical and Chemical Constants and Some Mathematical Functions* (London: Longman)
- [23] Tamaru K 1956 The thermal decomposition of tin hydride *J. Phys. Chem.* **60** 610–2
- [24] OECD and N. E. Agency 2012 *Chemical Thermodynamics of Tin* vol 12 (Paris: OECD Nuclear Energy Agency) pp 134–6
- [25] Ugur D, Storm A, Verberk R, Brouwer J and Sloof W G 2014 Decomposition of SnH₄ molecules on metal and metal-oxide surfaces *Appl. Surf. Sci.* **288** 673–6
- [26] Faradzhev N and Sidorkin V 2009 Hydrogen mediated transport of Sn to Ru film surface *J. Vac. Sci. Technol. A* **27** 306–14

- [27] Zaleski-Ejgierd P, Hoffmann R and Ashcroft N W 2011 High pressure stabilization and emergent forms of PbH_4 *Phys. Rev. Lett.* **107** 037002
- [28] Hein T A, Thiel W and Lee T J 1993 *Ab initio* study of the stability and vibrational spectra of plumbane, methylplumbane and homologous compounds *J. Phys. Chem.* **97** 4381–5
- [29] Lippert E 1960 The strengths of chemical bonds, von T. L. Cottrell. Butterworths Publications Ltd., London 1958. 2. Aufl., x, 317 s., geb.t—/32/— *Angew. Chem.* **72** 602
- [30] Wang X and Andrews L 2003 Infrared spectra of group 14 hydrides in solid hydrogen: experimental observation of PBH_4 , PB_2H_2 and PB_2H_4 *J. Am. Chem. Soc.* **125** 6581–7
- [31] Dean J and Lange N 1999 *Lange's Handbook of Chemistry* (New York: McGraw-Hill)
- [32] Ohchi T, Kobayashi S, Fukasawa M, Kugimiya K, Kinoshita T, Takizawa T, Hamaguchi S, Kamide Y and Tatsumi T 2008 Reducing damage to Si substrates during gate etching processes *Jpn. J. Appl. Phys.* **47** 5324–6
- [33] Park S and Walser R 1985 Hydrogen plasma etching of pyromeric carbon films *Carbon* **23** 701–6
- [34] Astakhov D I, Goedheer W J, Lee C J, Ivanov V V, Krivtsov V M, Yakushev O, Koshelev K N, Lopaev D V and Bijkerk F 2015 Numerical and experimental studies of the carbon etching in EUV-induced plasma (<https://doi.org/10.48550/arXiv.1507.02705>)
- [35] van Leuken D P J, de Meijere C A, van der Horst R, Banine V Y, Osorio E A and Beckers J 2021 An atomic hydrogen etching sensor for H_2 plasma diagnostics *Rev. Sci. Instrum.* **92** 063518
- [36] Hadjadj A, Larbi F, Gilliot M and Cabarrocas P 2014 Etching of a-Si:H thin films by hydrogen plasma: a view from *in situ* spectroscopic ellipsometry *J. Chem. Phys.* **141** 084708
- [37] Van Herpen M, Klunder D, Soer W, Moors R and Banine V 2010 Sn etching with hydrogen radicals to clean EUV optics *Chem. Phys. Lett.* **484** 197–9
- [38] Elg D, Panici G, Peck J, Srivastava S and Ruzic D 2017 Modeling and measurement of hydrogen radical densities of in situ plasma-based Sn cleaning source *Proc. SPIE* **16** 023501
- [39] Kuznetsov A S, Gleeson M A and Bijkerk F 2014 Temperature dependencies of hydrogen-induced blistering of thin film multilayers *J. Appl. Phys.* **115** 173510
- [40] Lawn B 1993 *Fracture of Brittle Solids* (Cambridge: Cambridge University Press)
- [41] Chase M 1998 *Nist-Janaf Thermochemical Tables* 4th edn (Gaithersburg, MD: National Institute of Standards and Technology)
- [42] Risold D, Nagata J and Suzuki R 1998 Thermodynamics of the Pb-O system *J. Phase Equilib.* **19** 213–33
- [43] Condon J and Schober T 1993 Hydrogen bubbles in metals *J. Nucl. Mater.* **207** 1–24
- [44] Ou W, Al R, Vernimmen J, Brons S, Rindt P and Morgan T 2020 Deuterium retention in Sn-filled samples exposed to fusion-relevant flux plasmas *Nucl. Fusion* **60** 026008
- [45] Kamada K 1989 Hydrogen implantation effects in the subsurface layer of aluminum -bubble pressure and surface modifications *J. Nucl. Mater.* **169** 141–50
- [46] Xie D-G, Wang Z-J, Sun J, Li J, Ma E and Shan Z-W 2015 *In situ* study of the initiation of hydrogen bubbles at the aluminium metal/oxide interface *Nat. Mater.* **14** 899–903
- [47] Smithells C J 2014 *Smithells Metals Reference Book* 8th edn, ed W F Gale and T C Totemeier (Woburn, MA: Butterworth-Heinemann)